Coupled high-resolution land-atmosphere modeling for hydroclimate and terrestrial hydrology in Alaska and the Yukon River basin (1990-2021)

Yifan Cheng[1,*], Anthony Craig[2], Keith Musselman[3], Andrew Bennett[4], Mark Seefeldt[5], Joseph Hamman[6], Andrew J. Newman[1]

1. Research Applications Laboratory, NSF National Center for Atmospheric Research, Boulder CO, USA
2. Contractor to the University of Colorado, Seattle WA, USA
3. Institute of Arctic and Alpine Research and Department of Geography, University of Colorado Boulder, Boulder CO, USA
4. Hydrology and Atmospheric Sciences, University of Arizona, Tucson AZ, USA
5. Cooperative Institute for Research in Environmental Sciences, University of Colorado Boulder, Boulder, CO, USA
6. Earthmover, Seattle WA, USA

* Corresponding to: Yifan Cheng (yifanc93@gmail.com)

Key points:

- Iterative testing was implemented to improve both hydroclimate and terrestrial hydrology simulations in coupled land-atmosphere models
- We generated a high-fidelity 4 km climate dataset (1990-2021) for Alaska and Yukon and evaluated it against multiple observational dataset
- Discrepancies in streamflow simulations between the offline land model and the coupled models were diagnosed using information theory

Abstract:
Hydroclimate and terrestrial hydrology greatly influence the local community, ecosystem, and economy in Alaska and Yukon River Basin. A high-resolution re-simulation of the historical climate in Alaska can provide an important benchmark for climate change studies. In this study, we utilized the Regional Arctic Systems Model (RASM) and conducted coupled land-atmosphere modeling for Alaska and Yukon River Basin at 4-km grid spacing. In RASM, the land model was replaced with the Community Terrestrial Systems Model (CTSM) given its comprehensive process representations for cold regions. The microphysics schemes in the Weather Research and Forecast (WRF) atmospheric model were manually tuned for optimal model performance. This study aims to maintain good model performance for both hydroclimate and terrestrial hydrology, especially streamflow, which was rarely a priority in coupled models. Therefore, we implemented a strategy of iterative testing and re-optimization of CTSM. A multi-decadal climate dataset (1990-2021) was generated using RASM with optimized land parameters and manually tuned WRF microphysics. When evaluated against multiple observational datasets, this dataset well captures the climate statistics and spatial distributions for five key weather variables and hydrologic fluxes, including precipitation, air temperature, snow fraction, evaporation-to-precipitation ratios, and streamflow. The simulated precipitation shows wet bias during the spring season and simulated air temperatures exhibit dampened seasonality with warm biases in winter and cold biases in summer. We used transfer entropy to investigate the discrepancy in connectivity of hydrologic fluxes between the offline CTSM and coupled models, which contributed to their discrepancy in streamflow simulations.

Plain Language Summary:
Hydrologic fluxes in the land-atmosphere interface, such as precipitation and streamflow, affect the local community, ecosystem, and economy in Alaska and Yukon River Basin. Therefore, we need a fine-grain historical dataset as a benchmark for climate change studies. We used a computer model, including an atmospheric and a land module, to generate a multi-decadal dataset for climate (1990-2021) at 4-km grid spacing. Before generating the dataset, we customized the computer model for Alaska and Yukon River Basin. We specifically implemented an iterative testing and re-modification strategy to make sure that our modification to either land or atmospheric modules would not worsen the overall model performance. To evaluate the dataset, in-situ measurements and satellite observations were used to evaluate five key weather variables and hydrologic fluxes, including precipitation, air temperature, snow fraction, evaporation-to-precipitation ratios, and streamflow. This dataset captures the quantity and seasonal variability of these variables very well, with slightly wet biases in spring, warm biases in winter and cold biases in summer. In addition, we used a statistical method, called transfer entropy, to study how the modification to the land module affects the modeled water cycles.

1 Introduction

The climate of Alaska, like much of the Arctic, is undergoing rapid change. Mean annual and seasonal air temperatures are increasing statewide with the largest warming signal detected in winter (Bieniek et al., 2014; Stafford et al., 2000). In response to warming, we have observed a large increase in the extent of permafrost degradation (Jorgenson et al., 2006; Lawrence & Slater, 2005; Osterkamp & Romanovsky, 1999; Saito et al., 2020), a shifted annual snow cycle and earlier snowmelt (Cox et al., 2017; Musselman et al., 2021; Stone et al., 2002), as well as increasing cold season discharge in Alaskan rivers (Blaskey et al., 2023; Gudmundsson et al., 2019). These hydroclimatic changes are deteriorating the quality of river ice roads and corresponding transportation safety, affecting terrestrial and aquatic ecosystems, and disproportionately increasing threats to Indigenous Alaskans, especially those who practice subsistence living (Knoll et al., 2019; McNeeley & Shulski, 2011). In Alaska the changes in magnitude and seasonality of precipitation exhibit larger uncertainties compared to temperature signals, with only the northern slope exhibiting a statistically significant increasing precipitation trend (Bieniek et al., 2014; White et al., 2021). An accurate accounting of the recent past along with improved process understanding can lay the foundation for improved resilience to extreme events and future climate change.

One frequently used tool to improve our process understanding and representation of regional climate are Regional Climate Models (RCMs). RCMs are widely used to reproduce historical weather and enable investigation of processes, potential changes, and subsequent impacts. Efforts such as CORDEX, NA-CORDEX, and Arctic CORDEX (Akperov et al., 2019; Gutowski Jr. et al., 2016; Mearns et al., 2017), have advanced our understanding of regional climate (Bukovsky et al., 2015; Cassano et al., 2017; Schär et al., 1996). Further, high-resolution RCMs at convection permitting, or complex orography resolving resolutions (e.g., grid spacings around or less than 5-10 km) have demonstrated many strengths in representing regional processes such as mesoscale convection systems (MCSs), seasonal snow cover and snow-albedo feedback, and the large-scale regional climate. This has been shown across domains such as the United States (Monaghan et al., 2018; Newman et al., 2021; Rasmussen et al., 2023; Xue et al., 2020); Canada (Li et al., 2019); and Europe (Berg et al., 2013).

RCMs without correction or tuning based on observations may lead to large biases that are critical to improve model simulation fidelity (e.g., Maraun, 2012). Tuning of RCMs has primarily centered around key atmospheric variables such as air temperature and precipitation (Bellprat et al., 2016; Wei et al., 2002). Specifically, parameterizations of cloud microphysics have frequently been the focal point (Bellprat et al., 2016; Couvreux et al., 2021; Wei et al., 2002) because of their strong impact on the surface energy and water budgets. Terrestrial hydrology and especially streamflow have been largely overlooked during RCM tuning. High-resolution RCMs are often used as weather models where the land model serves as a simpler lower boundary condition for short simulations. The development teams of RCMs are often led by atmosphere and ocean scientists that may lack hydrological expertise, thus prioritizing other critical issues such as cloud and precipitation biases. Particularly as RCMs are increasingly used to assess terrestrial ecosystems and water resources (Tapiador et al., 2020), we need to address the unique challenges related to land model and hydrology optimization in RCMs.

Optimizing component models in RCMs or coupled simulations is a multi-faceted challenge, particularly for hydroclimate and terrestrial hydrology. First, direct formal optimization such as algorithmic parameter sampling of coupled RCMs that includes multiple component models, is prohibitively expensive. Work-around efforts include using a statistical approximation of the climate model, using low spatial resolution, and limiting the number of parameters for optimization (e.g., Bellprat et al., 2012, 2016). While land models are comparatively less costly to optimize, the optimal parameters are strictly only applicable to the selected meteorological forcings. The terrestrial hydrology in the coupled simulation could degrade if the simulated meteorology in the RCM drifts significantly from the optimization climate. Standalone land model optimization fails to incorporate land-atmosphere interactions and the optimized land parameters may negatively impact the performance of the coupled RCM (Papadimitriou et al., 2017). Even after tuning, RCMs contain biases and errors that must be evaluated and clearly documented to provide sufficient contexts for all users to assess the adequacy of any particular simulation for their application.

The objective of this study is to maximize hydroclimate and terrestrial hydrology simulation performance in a land-atmosphere coupled RCM simulation for the Alaska and Yukon River Basin. We used the traditional approach of offline optimization of the land parameters, specifically for snow and streamflow (Cheng et al., 2023), and incorporated them back into the coupled modeling framework. Two measures were implemented to mitigate potential degradation of the coupled model simulation. First, the high-resolution dataset (Monaghan et al., 2018) used to generate meteorological forcing in the offline land optimization, was produced by the same atmospheric model as used in the RCM. Second, we applied an iterative testing and re-optimization of the land model to ensure satisfactory coupled model performance. Specifically, in the iterative testing, we evaluated the performance of the offline-optimized land parameters in the coupled model by running a coupled simulation at a coarser resolution. Eventually, a multi-decadal climate dataset (1990 to 2021) for Alaska and Yukon River Basin was generated at 4 km grid spacing using the coupled RCM and optimized land model parameters. We examined the key weather and surface hydrologic variables and explored the differences in streamflow simulation outcomes between the standalone and coupled simulations.

In the following text, Section 2 describes the coupled modeling framework, including optimization of the land model and configurations of the atmospheric model; Section 3 describes the study domain; Section 4 outlines proposed model evaluations against several observational datasets, and methods for diagnosing the discrepancies in streamflow simulations between standalone CTSM and coupled models; Section 5 presents results for the model evaluations and diagnoses; Sections 6 and 7 are discussions and conclusions respectively.

2 Model framework

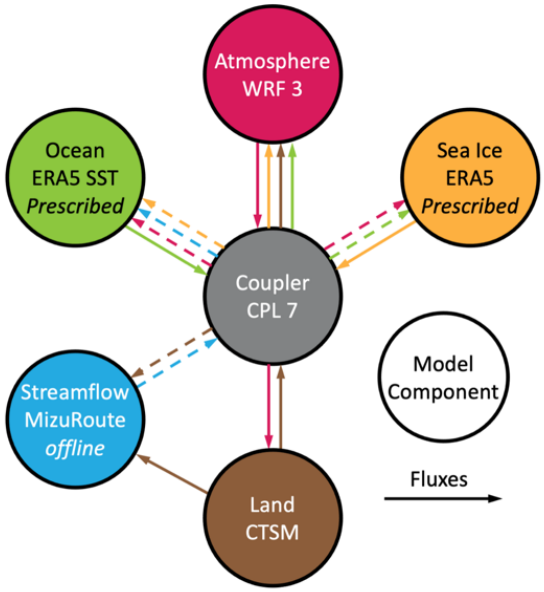

Figure 1. Model framework. Dashed arrows denote the fluxes that only exist in fully coupled RASM simulation but do not exist in this study.

2.1 Regional Arctic System Model (RASM)

We employed the Regional Arctic System Model (RASM), a limited-area and fully coupled land-atmosphere-ocean-sea ice and river routing model that uses the Community Earth System Model (CESM) framework (Cassano et al., 2017). Prescribed sea surface temperature (SST) and sea ice fraction data from the ECMWF Reanalysis v5 (ERA5, Hersbach et al., 2020) is used for the sea ice and ocean lower boundary conditions given the emphasis on the land-atmosphere interaction. In this study, the previously used land component model, Variable Infiltration Capacity model (VIC, Hamman et al., 2016), was substituted with the Community Terrestrial Systems Model (CTSM). CTSM incorporates comprehensive land processes representations, including complex vegetation and canopy modules, a multi-layer snow model, and hydrology and frozen soil physics (Lawrence et al., 2019). Streamflow was routed offline using mizuRoute (Mizukami et al., 2016). Our modifications to the default RASM configuration are depicted in Figure 1, with dashed arrows representing the flux communication unique to the default configuration and not present in this study.

2.1.1 Generating a historical multi-decadal climate dataset for Alaska and Yukon River Basin

We generated a multi-decadal climate dataset (1990 to 2021) at 4 km grid spacing for Alaska and Yukon River Basin by running RASM with the optimized land parameters (Section 2.2) and manually tested WRF configurations (Section 2.3). The model simulation started from June 1, 1989 and ended on September 30, 2021 with the first model year as spin-up. This is a tremendous computational undertaking that costs nearly 10 million CPU hours with roughly 300 thousand CPU hours per model year.

For the land model, a total of 275 variables were saved at 3-hourly, daily, or monthly timesteps. For the atmospheric model, a total of 265 variables were saved at hourly, 6-hourly, or daily timesteps. The total data volume is roughly 55 TB. More details about this climate dataset can be found in the data archive document (Cheng et al., 2024).

2.2 Offline optimization for Community Terrestrial Systems Model (CTSM)

We conducted an offline optimization for CTSM to increase the fidelity of terrestrial hydrologic simulations. Given that CTSM is computation-intensive compared to most hydrological models, we utilized a computationally frugal machine learning technique, i.e., a surrogate modeling-based optimization method (Wang et al., 2014), and selected smaller sub-basins as representatives for optimization to offset some computational expenses. A regionalization method was applied to extrapolate the optimized parameters from the representative basins to the entire domain. The details concerning the optimization are presented in Cheng et al (2023). As we briefly discussed in Introduction, two measures were implemented to ensure satisfactory coupled model behavior.

First measure aims to ensure the simulated climatology in the coupled model will not drift away from the one used in land model optimization. For our study region, a previous historical simulation using a similar version of WRF with ERA-Interim forcing data exists (Monaghan et al., 2018) and we used it as the meteorological forcings in the land model optimization. Even so, it is also important to acknowledge that Monaghan et al (2018) used a slightly older version of WRF, ERA-Interim, and the Noah-MP land model, while we used a newer version of WRF, ERA5, and the CTSM land model.

Second, we applied an iterative testing and re-optimization strategy. In each iteration, we examined the performance of coupled simulations with optimized land parameters at a coarser 12 km spatial resolution by comparing them with the hydrologic and energy fluxes in ERA5. When model performance of coupled simulations was not satisfactory, we diagnosed the reason, made corresponding modifications to the parameters, and re-optimization. An example iteration is showcased below.

In one iteration, *medlynintercept*, a parameter governing stomatal conductance (Kennedy et al., 2019), approached the upper limit (300,000) in the optimization. The coupled simulations using this set of optimized parameters show excessive summer evaporation, elevated cloud coverage, and a domain-wide -4.64°C cold bias in 2-meter summertime (June-August 2013) air temperature compared to ERA5 (Figure 2). The parameter range for *medlynintercept* was originally established by experts for global-scale studies, which may require refinement for regional applications (Kennedy et al., n.d.). Consequently, our use of the unconstrained parameter range introduced compensatory errors that may not be apparent during offline optimization. Correspondingly, by reducing the upper limit for *medlynintercept*, i.e., 20,000, the performance of the coupled model showed marked improvement with minimal impact on the offline model performance. This again highlights the need for iterative testing, technical knowledge of the models and parameterizations, and clear documentation across those models and parameterizations (Jakob, 2010).

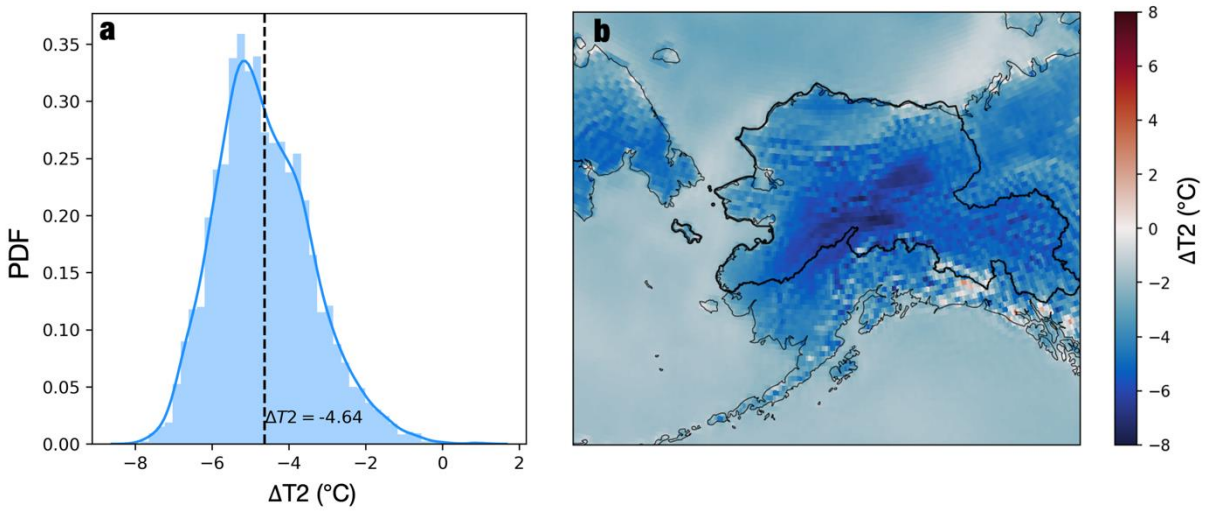

Figure 2: Initial bias of 2-meter summer air temperature (ΔT2) in the RASM simulation using offline optimized CTSM parameters (with large *medlynintercept* value) compared with ERA5 reanalysis data. Panel (a) shows the distribution of ΔT2 across all grid cells in the domain and panel (b) shows the spatial distribution of ΔT2

2.3 Configuring the Weather Research and Forecasting (WRF) Model

The atmospheric model in RASM is a modified version of the Advanced Research WRF (WRF-ARW, hereafter simply WRF) Model version 3.7.1 (Cassano et al., 2017; Skamarock et al., 2008). The selection of physics options was informed by an earlier high-resolution WRF simulation for Alaska (Monaghan et al., 2018) as well as RASM pan-arctic simulations (Cassano et al., 2017). While Monaghan et al (2018) utilized the Noah-MP land model integrated in WRF, this study employed CTSM as the land model. Therefore, we performed manual testing of different physics options and summarized the final selection in Table 1. We selected the MYNN level 2.5 scheme (Janić, 2001) whereas Monaghan employed the Yonsei University (YSU) scheme (Hong et al., 2006). In addition, we used a newer version of the ECMWF Reanalysis data, ERA5, as the initial and lateral boundary conditions, SST, and sea ice fraction while Monaghan et al. (2018) used ERA-Interim.

Table 1: List of WRF options used in the RASM simulation

WRF version Horizontal grid spacing	3.7.1 4 km
Horizontal grid points	782 longitude (x) grid × 662 latitude (y) grid
Number of vertical levels /model top	49/30hPa (7 levels in the lowest 1000 m)
Time step	WRF: 20 s WRF radiation: 10 min RASM coupler: 10 min
Lateral BCs	ERA5
Longwave radiation	RRTMG
Shortwave radiation	RRTMG
Cloud microphysics	Thompson
Planetary boundary layer	MYNN level 2.5 schemes
Cumulus	Off

3 Domain

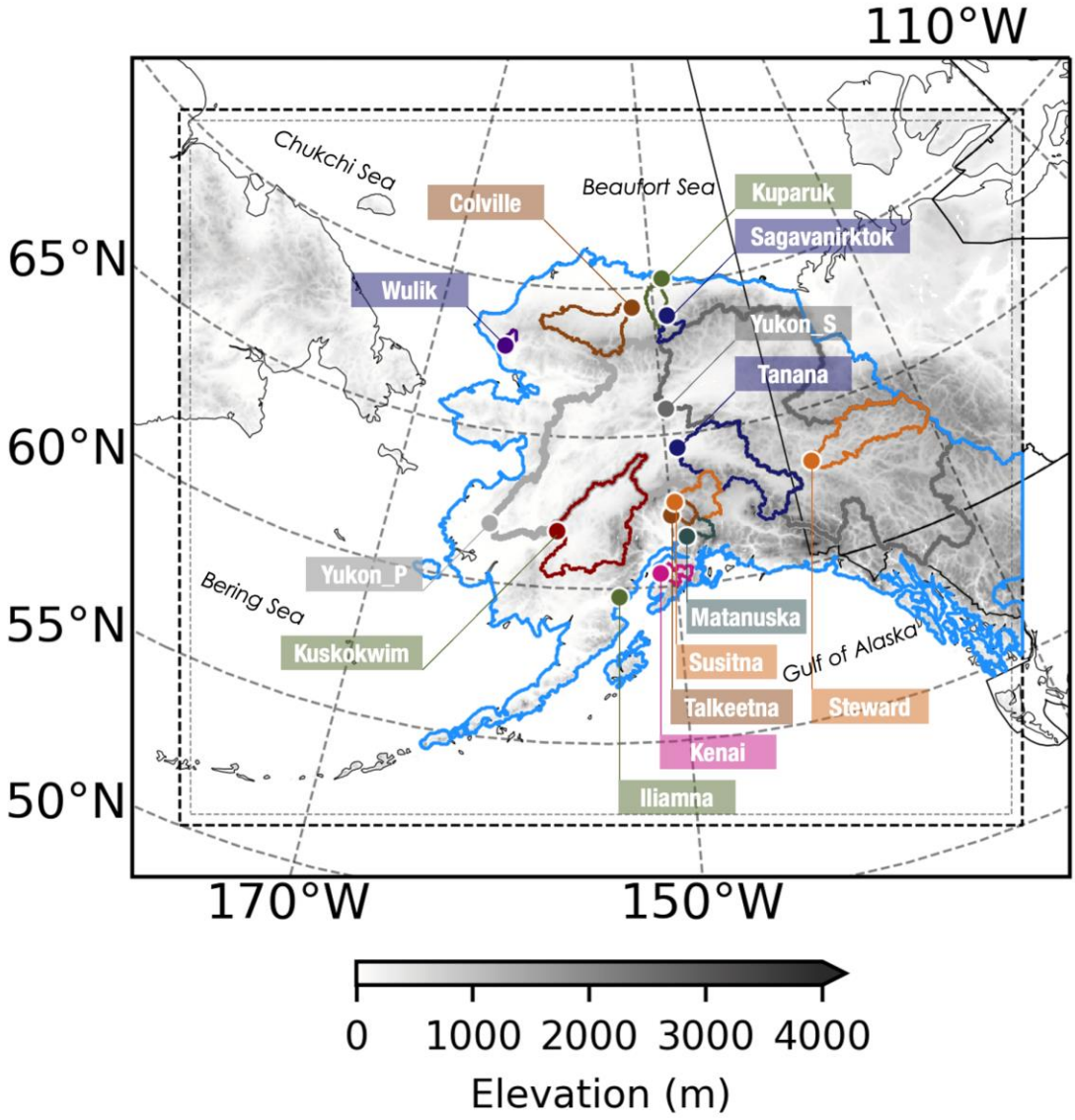

Figure 3. Study domain

In the coupled WRF-CTSM modeling, the terrestrial domain defined by the black dashed box in Figure 3 encompasses nearly all the U.S. State of Alaska, the entire Yukon River Basin, part of Western Canada, and the eastern coastal region of Russia. The marine bodies consist of the Gulf of Alaska, Bering Sea, Chukchi Sea, and Beaufort Sea. The evaluation domain encompasses all land grid cells, delineated by light blue boundaries, given our research emphasis on land-atmospheric interactions. This evaluation domain is derived from the probabilistic spatial meteorological estimates specifically designed for Alaska, developed by Newman et al. (2020), which also serves as an observational dataset used for evaluation purposes. Consistent with Cheng (2023), we evaluated the streamflow simulation against observations for 15 major rivers depicted by solid colored lines. Yukon_S and Yukon_P denote two U.S. Geological Survey (USGS) gauges along the main stem of the Yukon River, located near Stevens Village and Pilot Station, respectively.

4 Model evaluation

We conducted a comprehensive evaluation of the generated climate dataset for hydroclimate and terrestrial hydrology, including the assessment of five weather variables and hydrologic fluxes (Section 4.1). The evaluated variables are precipitation, 2-meter air temperature, snowfall fraction (S/P, representing the ratio of snowfall to precipitation), evaporation precipitation ratio (E/P), and streamflow. In order to examine the robustness of standalone CTSM optimization within the coupled model, we compared the simulated streamflow obtained from the coupled model with that from standalone CTSM optimization. Moreover, to elucidate the disparities between the two streamflow simulations, we conducted in-depth analyses encompassing: 1) assessment of the meteorological drivers, 2) investigation of the interdependencies among hydrologic fluxes using transfer entropy, and 3) exploration of climate sensitivities to streamflow.

4.1 Observational Dataset

Table 2: Summary of datasets used for evaluation.

Variable	Observation/Reanalysis Dataset	Evaluation Period
Precipitation	Probabilistic Spatial Meteorological Estimates (PSME, Newman et al 2020)	1990-2013
	Global Precipitation Climatology Project (GPCP, Satellite-derived precipitation data)	1990-2020
	PNWNAmet (Gridded interpolation from observation)	1990-2012
2-m air temperature	Probabilistic Spatial Meteorological Estimates (PSME, Newman et al 2020)	1990-2013
	Site observation (507 sites)	Varying
Evaporation Precipitation Ratio (E/P)	ERA5	1990-2021
Snowfall fraction (S/P)	ERA5	1990-2021
Streamflow	USGS sites	Varying

Three gridded datasets were employed as benchmarks to evaluate precipitation (Table 2). Probabilistic Spatial Meteorological Estimate (PSME) was generated using the ensemble Climatologically Aided Interpolation (eCAI) for Alaska and the Yukon Territory (Newman et al., 2020). The eCAI method develops a probabilistic estimate of the climatological fields such as precipitation and air temperature and then develops daily values using daily anomalies. Note we use the uncorrected precipitation from the PSME product. The Global Precipitation Climatology Project (GPCP) provides monthly analysis of global precipitation from an integration of various satellite data sets (Adler et al., 2003). The PCIC meteorology for Northwest North America (PNWNAmet) is a gridded dataset generated using the trivariate thin plate spline interpolation method from observations (Werner et al., 2019). These three datasets were developed using different approaches and have served as benchmarks for evaluating precipitation simulation in other studies (Behrangi et al., 2016; Van Tiel et al., 2021).

Observations from 507 sites across Alaska were utilized for evaluating air temperature simulations, except for the PSME dataset. E/P and S/P ratios are both compared to the ERA5, given the limited data availability for evaporation and snowfall.

Streamflow simulation for the 15 major river basins were evaluated against the gauge measurement from USGS and the Department of Environment and Natural Resources in Canada. Nash Sutcliffe Efficiency (NSE) and Kling Gupta Efficiency (KGE) were calculated using daily streamflow data. It is worth noting that in Alaska, rivers freeze during the cold seasons, and to ensure a continuous time series, USGS provides streamflow estimates for frozen rivers denoted with a qualifier of "*Ae*". Therefore, we calculate the metrics specifically for free-flowing rivers during ice-free periods, and refer to them as NSE_w, KGE_w. Additionally, metrics were calculated for the entire available time series, denoted as NSE_a and KGE_a.

4.2 Diagnosing discrepancies in streamflow simulations between offline CTSM and the coupled model

Flow simulations between the offline CTSM optimization and coupled RASM model exhibit discrepancies. Since the land component of RASM is also CTSM, the discrepancy in streamflow simulation is likely driven by meteorological conditions. Six variables were analyzed, including three temperature and energy variables (2m air temperature, incident longwave and shortwave radiations), and three hydrologic fluxes (precipitation, evaporation, and snowmelt). These six variables are shown for inter-model comparisons.

We also investigate how the coupled model affects the response of runoff simulation (R) to changes in precipitation (P) and air temperature (T). We examined the runoff climate sensitivity of two modeling systems: CTSM and RASM, along with the widely used ERA5 reanalysis dataset. ERA5 sensitivity was solely used as a reference rather than a ground truth in this study. We followed the technique developed in Wood et al (2004). Regionally averaged precipitation ($\bar{P}$), air temperature ($\bar{T}$), and runoff ($\bar{R}$) were calculated for each hydrologic year in the RASM, CTSM, and ERA5 datasets. We conducted bootstrapping (n = 1,000 times) to quantify the uncertainties in runoff responses to climate variables. Each bootstrapping sample generated a new series of precipitation, air temperature, and runoff by resampling the available hydrological years with replacement. For each new series, we performed a simple linear regression between the streamflow and climate variables, with the slope representing the corresponding responses. The runoff sensitivity to precipitation (θ_P) is unitless and the unit for runoff sensitivity to air temperature (θ_T) is mm day^{-1} °C^{-1}. Additionally, we calculated the correlation coefficient between the streamflow and climate variables, denoting as ρ_P and ρ_T, which indicated the uncertainties in the corresponding responses of precipitation and air temperature, respectively.

The connectivity between the energy and hydrologic fluxes can change because the coupled model captures the two-way interactions between the land surface and the atmosphere. To quantify the transfer of information between these processes across different modeling systems, we employed an information theoretic measure, i.e., transfer entropy (Bennett et al., 2019; Schreiber, 2000). Transfer entropy provides a statistical measure of how much uncertainty about a current process can be reduced by knowledge of the history of another variable (taking the target process's history into account). Eight weather and hydrologic variables and flux terms were analyzed: 2m air temperature, incident longwave and shortwave radiations, runoff,

evapotranspiration, precipitation, snow water equivalent (SWE), and soil moisture (SM). Since the SWE and SM are state variables, we used daily changes in SWE and SM, denoting as ΔSWE and ΔSM and all other variables are daily averages. Evapotranspiration in CTSM and RASM were split into soil evaporation and canopy evapotranspiration whereas ERA5 only provides the total evapotranspiration. ERA5 provides soil moisture for the top four soil layers with a total depth of 2.89 m whereas CTSM and RASM provide soil moisture for 20 soil layers with a total depth of 8.03 m. Rather than using soil moisture for entire soil columns, we used the surface soil moisture (7 centimeters for ERA5 and 9 centimeters for CTSM and RASM) to ensure that the results between ERA5 with CTSM and RASM were comparable.

For simplicity, we used a single-variate approach and calculated lag-1 day transfer entropy. It is important to note that the process connectivity presented in this study is limited by the selected method. Multivariate process connectivity and the process connectivity at different temporal scales are not considered due to unreliability of calculating higher-dimensional probability distributions (Hlaváčková-Schindler et al., 2007). The transfer entropy for each pair of variables is calculated at a daily time scale using a formulation of lag 1 transfer entropy, with lag 1 representing a single day (Eqn. 1).

$$T_{X \to Y} = I(Y_t; X_{t-1} | Y_{t-1}) \qquad \text{Eqn. 1}$$

where $T_{X \to Y}$ is the transfer entropy from X to Y and the current state of Y_t depends only on the previous time step (i.e., X_{t-1} and Y_{t-1}). I denotes the conditional mutual information and the details concerning calculations can be referred to Bennett et al (2019). To ensure robustness of the estimated transfer entropy, we conducted bootstrapping (n=50, sample size=5000). We only report results which are significant at a 99% confidence level according to a shuffled surrogate test, which compares the transfer entropy of the true time series against the transfer entropy where the data has been shuffled, removing any temporal correlations (Marschinski & Kantz, 2002).

We conducted this analysis over the largest river basin, the Yukon River at Pilot Station. The time series of all grid cells located in its confluence area were averaged to get one representative time series for this region.

5 Results

In the following section, RASM denotes the coupled model simulation and CTSM denotes the offline land-only simulation.

5.1 Model evaluation against observational datasets

The simulated historical climate means of precipitation and temperature are shown in Figure 4. The high-resolution RASM captures the orographic impacts and complex ridge-valley patterns on the spatial distribution of precipitation and air temperatures. Notably, this modeling effort also exhibits the spatial heterogeneity of precipitation between the windward and leeward sides of the Aleutian Islands.

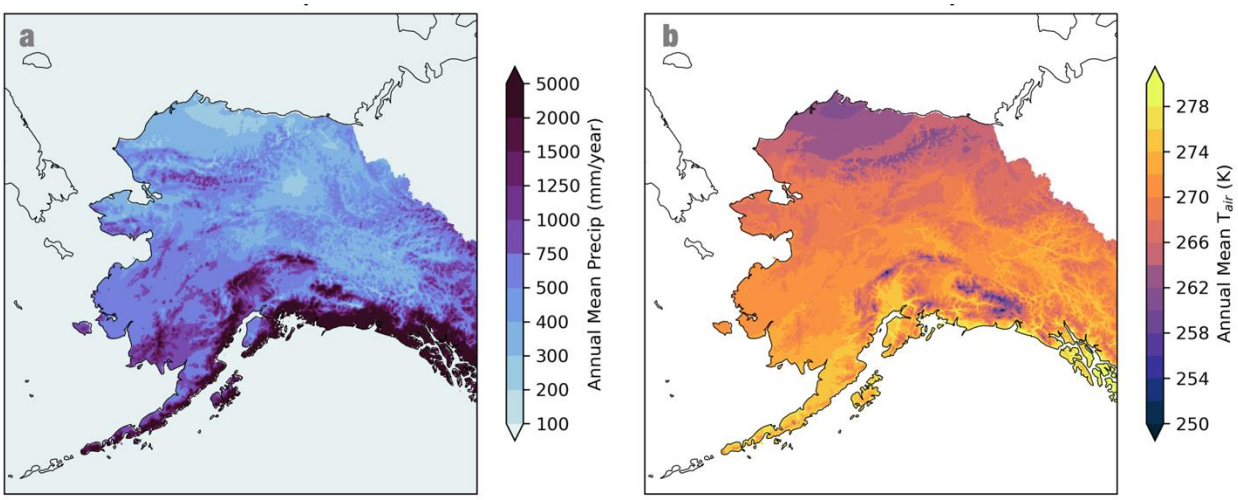

Figure 4. Simulated mean annual precipitation (a) and air temperature (b) for WY 1990-2021.

Table 3: Spearman rank-order correlation coefficient between RASM and evaluation datasets and median relative biases across the entire evaluation domain.

	Spearman Correlation Coefficient					Median relative bias across domain				
	Annual	Winter	Spring	Summer	Fall	Annual	Winter	Spring	Summer	Fall
PNWNAmet	0.86	0.82	0.79	0.77	0.85	14.4%	10.4%	37.2%	8.0%	11.3%
GPCP	0.74	0.73	0.74	0.56	0.75	16.7%	10.0%	28.8%	20.0%	11.3%
PSME-mean	0.78	0.72	0.73	0.68	0.79	32.9%	21.2%	69.4%	21.4%	37.9%
PSME-75prct	0.78	0.72	0.74	0.67	0.79	-2.1%	-11.4%	27.4%	-11.0%	-0.1%

5.1.1 The spatial pattern and quantify of precipitation are well simulated

The high-resolution RASM well simulates the spatial distribution and quantity of precipitation in Alaska and the Yukon region. For annual mean precipitation, the Spearman rank-order correlation coefficients between RASM and the evaluation datasets are 0.86, 0.74, 0.78 for PNWNAmet, GPCP, and PSME-mean, respectively. The result is comparable to Monaghan et al (2018) and the high correlation coefficient indicates well-simulated spatial pattern of precipitation. Across the entire domain, the median relative biases in mean annual precipitation are 14.4% and 16.7% as compared to PNWNAmet and GPCP respectively (Table 3). When

compared with the PSME dataset, the RASM simulation falls between the ensemble mean and the 75 percentile (Table 3). Notably, RASM consistently overestimates precipitation in spring (March, April, May), the season with the lowest precipitation in Alaska, across all evaluation datasets (Table 3). Relatively large biases are observed in the southern coastal and mountainous ranges, where the three observation-based datasets display conflicting biases. Specifically, PSME and PNWNAmet suggest RASM consistently underestimates precipitation across all seasons while GPCP consistently indicates overestimation. Furthermore, GPCP shows that RASM underestimates spring precipitation in the Yukon headwater region and summer (June, July, August) precipitation in northern coastal region, whereas the PSME and PNWNAmet indicate the opposite. These inconsistencies highlight the significant uncertainties in precipitation data for Alaska, which remains a challenge for the scientific community and applications.

Figure 5d presents the distribution of seasonal biases against the 25th, 50th, 75th percentiles, as well as the mean of the PSME ensemble. The regional median biases for PSME ensemble means are 5.17 mm/season, 10.47 mm/season, 12.72 mm/season, 13.79 mm/season for winter (December, January, February), spring, summer, and fall (September, October, November), respectively. The regional median biases against the three PSME percentiles are slightly higher than 0, suggesting that the simulated precipitation has slight wet biases. Among the three datasets, PNWNAmet exhibits the closest resemblance to our simulated precipitation, with regional median biases of 2.77 mm/season, 6.81 mm/season, 5.06 mm/season, 4.91 mm/season for winter, spring, summer, and fall, respectively. Additionally, RASM consistently overestimates precipitation compared to the GPCP dataset, especially in summer season, with regional median biases of 2.83 mm/season, 5.76 mm/season, 11.74 mm/season, 4.99 mm/season for winter, spring, summer, and fall, respectively.

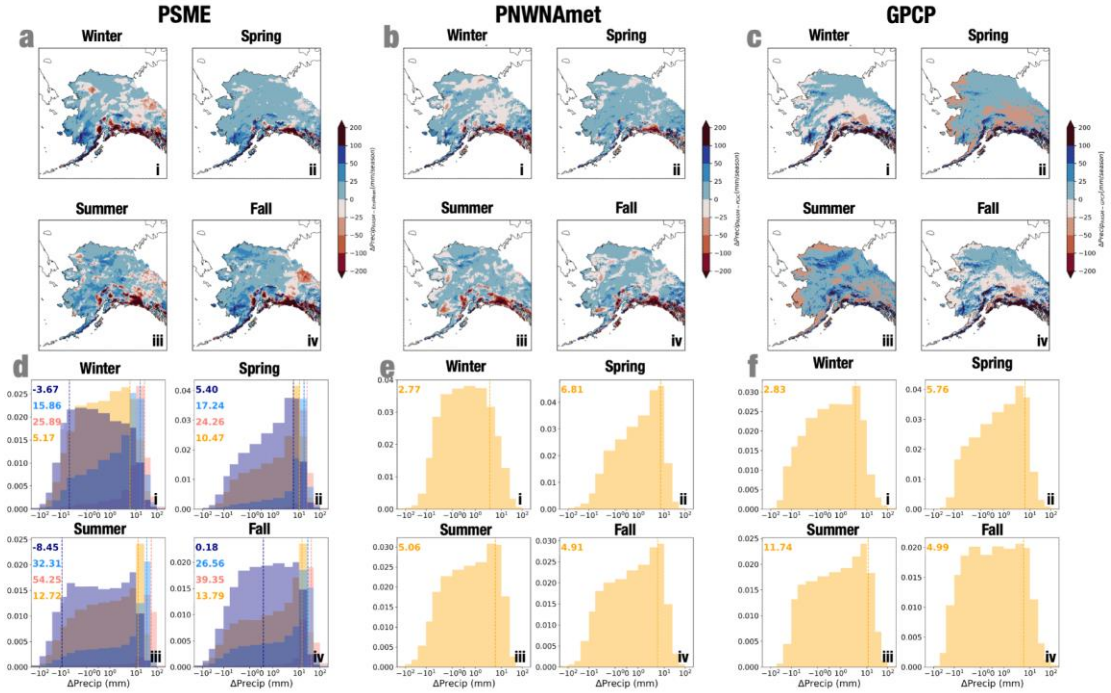

Figure 5. Evaluation of precipitation simulation against three datasets, i.e., PSME (Panels *a*,*d*), PNWNAmet (Panels *b*,*e*), and GPCP (Panels *c*,*f*). Panels *a*, *b*, and *c* show the spatial maps of mean seasonal bias. Panels *d*, *e*, and *f* show the distribution of seasonal biases across all grid cells with the

evaluation domain, with Panel *d* showing the seasonal biases against the 25th, 50th, 75th percentiles and mean of PSME ensemble. Vertical lines in panels d, e, and f denote median values across all grid cells. Sub-panels *i*, *ii*, *iii*, and *iv* denote winter, spring, summer, and fall.

5.1.2 Seasonality of temperature simulation is dampened in RASM

Simulated air temperature exhibits dampened seasonality compared to observations. The coupled model tends to overestimate winter temperatures while underestimating spring and summer temperatures. The regional averaged biases for the PSME ensemble means are 1.72°C, -1.74°C, -2.36°C, -0.28°C for winter, spring, summer, and fall, respectively, with the regional averaged biases against all three PSME percentiles < 0 (Figure *6d*). In situ observations exhibit comparable seasonal biases, with regional averaged biases of 1.99°C, -1.25°C, -0.66°C, 0.59°C for winter, spring, summer, and fall, respectively.

The biases in air temperatures display seasonal and spatial heterogeneities. The significant warm biases during winters are predominantly observed in the North Slope, southeast interior Alaska, and the Yukon headwaters (Figures *6a,i*, *6b,i*). However, the cold biases during summers are mostly observed in the north and west coast of Alaska. Additionally, the root mean square errors (RMSE) were calculated for each observational site with the mean value of 3.81°C. It is noteworthy that the sites with large RMSEs (Figure 6c) correspond with the sites with large winter biases (Figure 6*b,i*), suggesting that the winter warm biases are the primary errors in the temperature simulations.

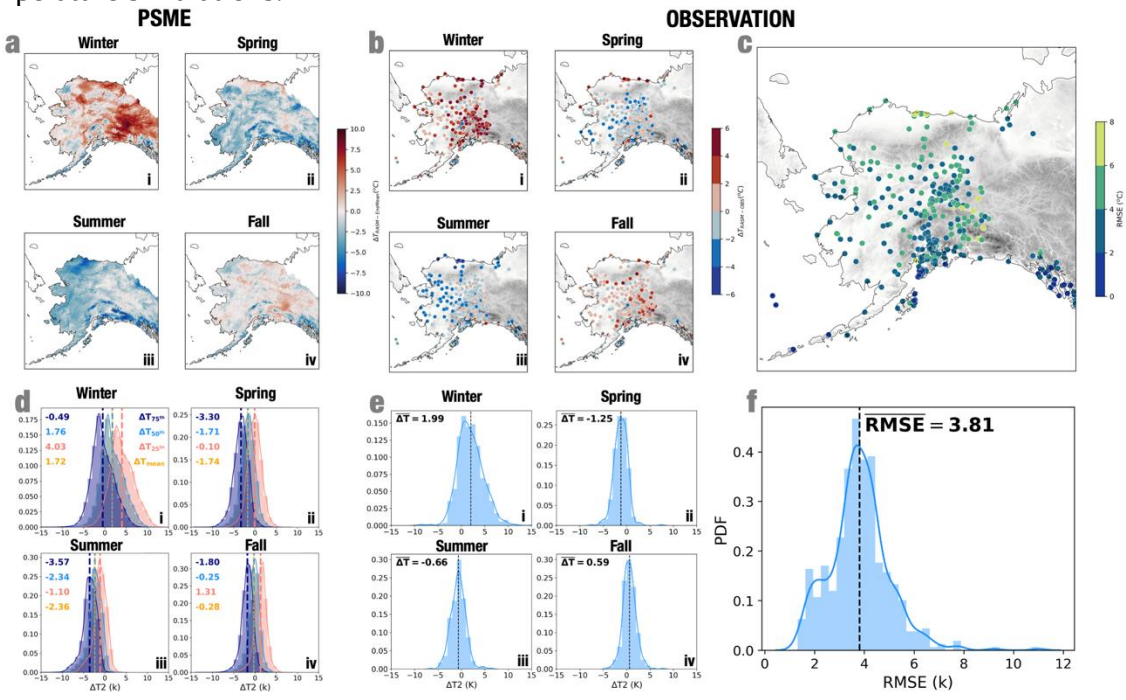

Figure 6. Evaluation of air temperature simulation against PSME (Panels *a*, *d*) and onsite observations (Panels *b*, *c*, *e*, *f*). Panels *a* and *b* show the spatial map of mean seasonal bias. In Panel *a*, it was evaluated against PSME ensemble mean. Panels *d* and *e* show the distribution of seasonal biases across all grid cells within the evaluation domain, with Panel *d* showing the seasonal biases against the 25th, 50th, 75th percentiles and mean of the PSME ensemble. Panels *c* and *f* show the spatial map and distribution of RMSE across all observational sites, respectively. Sub-panels *i*, *ii*, *iii*, and *iv* denote winter, spring, summer, and fall.

5.1.3 Snowfall fraction (S/P ratio)

The RASM simulation exhibits the spatial patterns of S/P ratios that generally resemble those observed in ERA5 for each season (Figures *7b* and *7c*). However, the simulated S/P ratio in RASM captures more realistic topographic details compared to ERA5 due to its higher spatial resolution. In addition, the regional averages of seasonal S/P ratios from RASM (ERA5) are 0.94 (0.94), 0.71 (0.64), 0.07 (0.04), and 0.58 (0.54) for winter, spring, summer, and fall, respectively. The slightly higher S/P ratio in RASM compared to ERA5 likely results from the higher spatial resolution of RASM, which enables the simulation to account for precipitation falling as snowfall over high mountainous regions during warm seasons.

5.1.4 Evaporation precipitation ratio (E/P ratio)

The RASM simulation shows greater variability in E/P ratios compared to ERA5. At the seasonal level, the regional averaged E/P ratios are similar, with values of -0.02 (0.02), 0.55 (0.58), 0.77 (0.74), and 0.20 (0.20) in RASM (ERA5) for winter, spring, summer, and fall, respectively. However, there are notable differences in their spatial patterns and distributions, which can be partially attributed to the discrepancies in spatial resolutions. RASM, with its high-resolution topography, results in more low-elevation grid cells having higher E/P ratios during the spring and summer seasons compared to ERA5. This rightward shift in the E/P ratio distribution can be observed in Figures *8a,ii* and *8a,iii*. However, the E/P ratios in the north and western coasts of Alaska are lower in RASM than in ERA5, which cannot be explained by the discrepancies in spatial resolution.

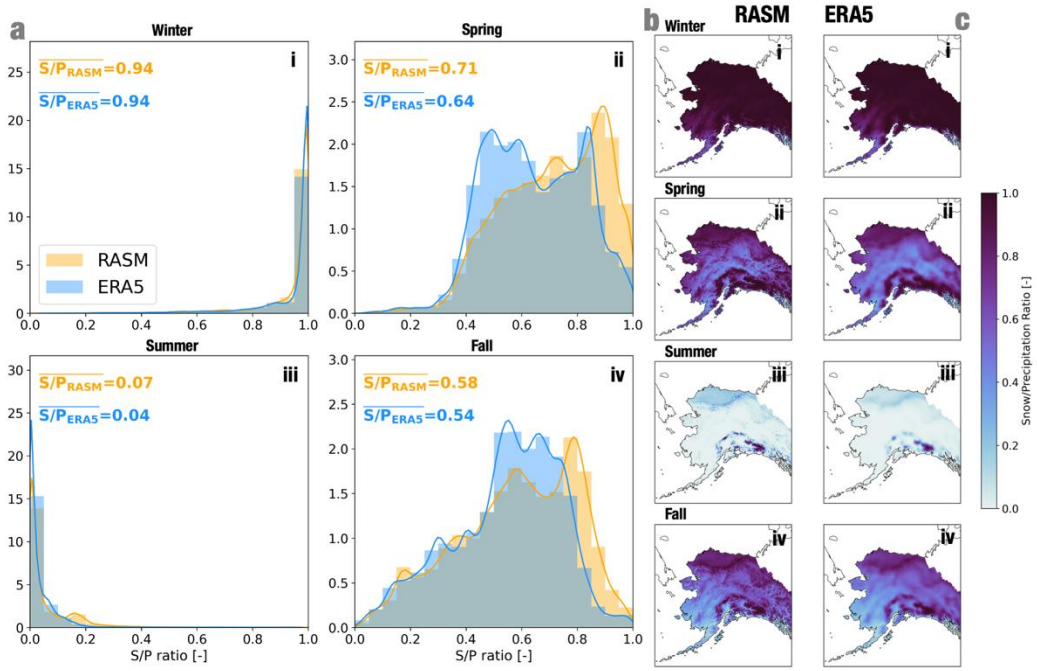

Figure 7. Evaluation of simulated S/P ratio against ERA5 dataset. Panel *a* shows the distribution of mean seasonal S/P ratio across all grid cells within the evaluation domain for RASM (orange) and ERA5 (blue), respectively. Panels *b* and *c* show the map of mean seasonal S/P ratio for RASM and ERA5, respectively.

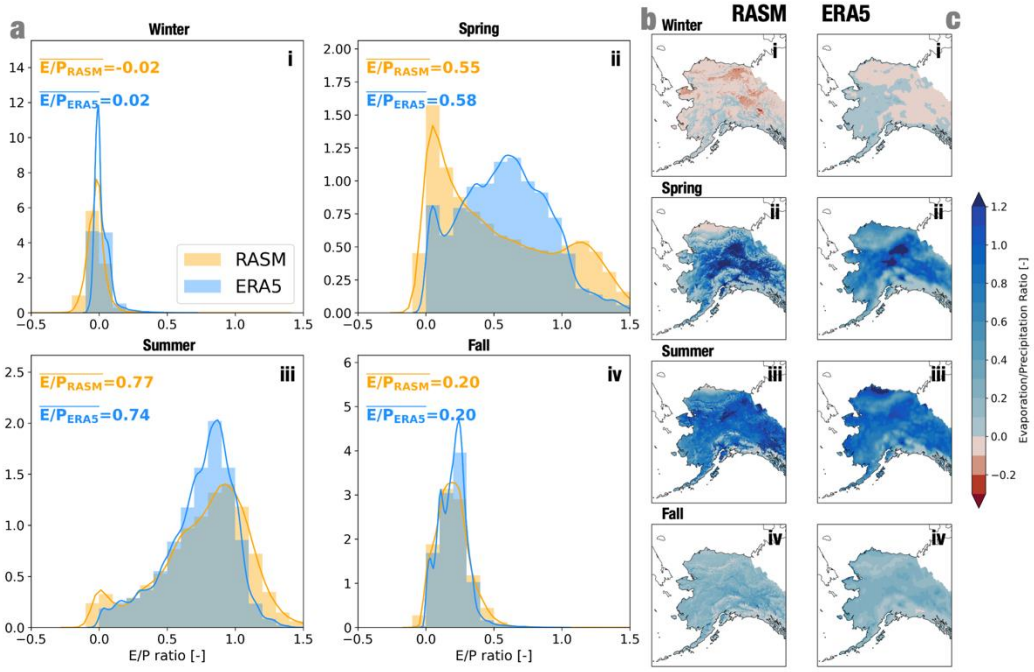

Figure 8. Similar to Figure 6 but for evaporation precipitation ratio (E/P).

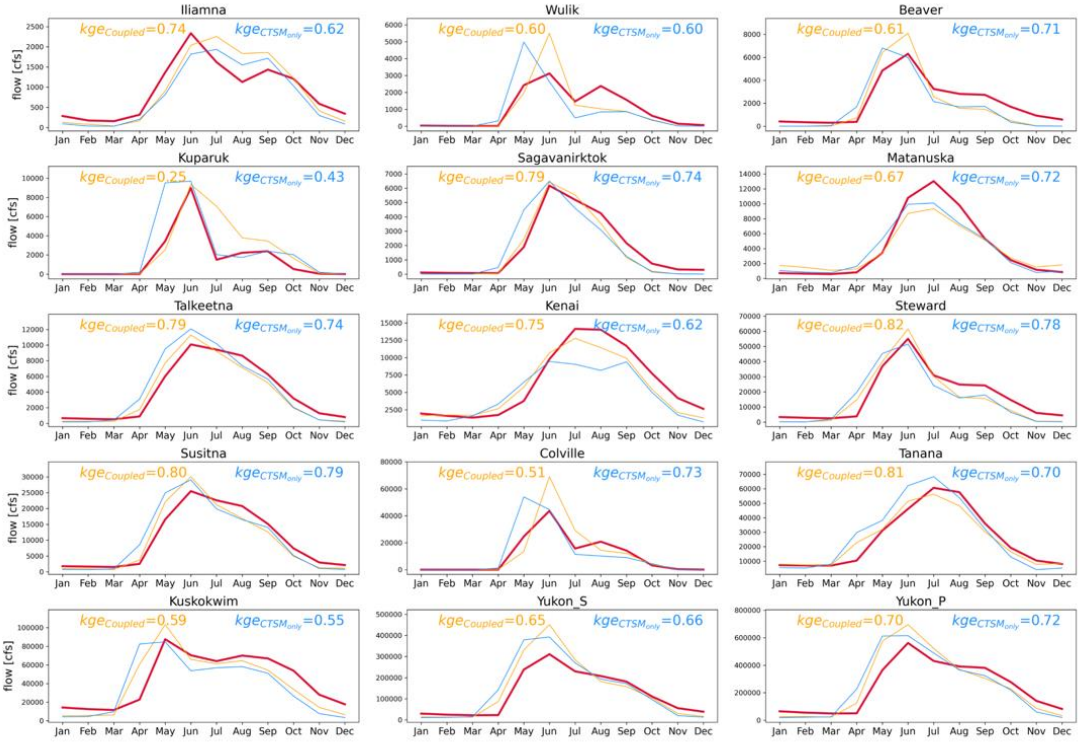

Figure 9. Evaluation of RASM streamflow simulation (orange) against USGS observations (red) and streamflow simulation in standalone CTSM optimization (blue)

Table 4: Summary of streamflow performances using Nash-Sutcliffe Efficiency and Kling-Gupta Efficiency.

	Nash Sutcliffe Efficiency				**Kling Gupta Efficiency**				**Nation**	**Number of Free-flowing days per year**
	NSE_a Entire period		NSE_w Warm Period		KGE_a All period		KGE_w Warm Period			
	RASM	CTSM	RASM	CTSM	RASM	CTSM	RASM	CTSM		
Iliamna	**0.49**	0.32	**0.37**	0.14	**0.74**	0.62	**0.69**	0.51	US	230
Wulik	0.17	0.25	-0.34	0.23	0.61	0.61	0.43	0.52	US	133
Beaver	0.51	0.51	0.51	0.51	0.61	0.71	0.61	0.71	Canada	
Kuparuk	0.13	0.35	-0.31	0.58	0.26	0.44	-0.05	0.68	US	117
Sagavanirktok	**0.62**	0.53	0.21	0.28	**0.80**	0.75	**0.63**	0.61	US	118
Matanuska	0.47	0.59	0.30	0.43	0.67	0.72	0.59	0.63	US	216
Talkeetna	**0.65**	0.55	**0.24**	0.10	**0.79**	0.75	**0.62**	0.59	US	174
Kenai	**0.50**	0.43	**0.30**	0.17	**0.75**	0.62	**0.67**	0.54	US	242
Steward	**0.71**	0.64	**0.71**	0.64	**0.81**	0.78	**0.81**	0.78	Canada	
Susitna	**0.70**	0.61	0.18	0.19	**0.80**	0.79	0.55	0.60	US	162
Colville	0.00	0.47	-0.49	0.57	0.51	0.73	0.29	0.75	US	132
Tanana	**0.61**	0.56	**0.14**	0.07	**0.81**	0.70	**0.60**	0.51	US	159
Kuskokwim	**0.22**	0.03	0.05	0.09	**0.60**	0.55	0.53	0.66	US	158
Yukon_S	**0.58**	0.50	0.18	0.55	0.65	0.66	0.50	0.72	US	159
Yukon_P	**0.60**	0.50	0.03	0.55	0.70	0.72	0.40	0.70	US	134
Median Value	***0.51***	***0.50***	***0.18***	***0.28***	***0.70***	***0.71***	***0.59***	***0.63***		

5.1.5 Streamflow evaluation

RASM provides generally good historical streamflow simulations with median NSE_a and KGE_a values of 0.51 and 0.70 across 15 major river basins (Table 4, Figure 9). This performance is comparable to the streamflow simulations achieved through standalone CTSM optimization, which yielded median NSE_a and KGE_a values of 0.50 and 0.71, respectively. Across the 15 basins, the NSE_a values all exceed 0 and KGE_a values exceed -0.41, indicating that RASM improves upon the mean streamflow benchmark (Knoben et al., 2019). Like Cheng et al (2023), we adopted a benchmark of daily NSE of 0.5 (Moriasi et al., 2015) and 9 out of 15 basins exceed this benchmark, showing comparable performance to the offline CTSM optimized simulation (Table 4). Notably, RASM shows improvements in streamflow simulations for 10 out of 15 basins based on NSE_a and 8 out of 15 basins based on KGE_a. The two exceptions are Yukon_S and Yukon_P, where RASM has KGE_a values of 0.65 and 0.70 respectively, only slightly lower than the corresponding KGE_a value of 0.66 and 0.72 obtained from CTSM. To our knowledge, this type of evaluation and performance may be unprecedented compared to other large regional land-atmosphere coupled RCM simulations.

Compared to CTSM, the RASM streamflow simulation shows a noticeable decline in performance during ice-free periods. The median NSE_w and KGE_w values across all 15 river basins are 0.18, and 0.58, respectively. These values are generally lower than the corresponding NSE_w and KGE_w values of 0.28 and 0.63 obtained from CTSM. Notably, when compared to CTSM, RASM exhibits improvements in streamflow simulations during warm seasons for only 5 out of 15 basins based on NSE_w and 6 out of 15 basins based on KGE_w. This highlights the challenges of translating offline optimization to coupled model problems and supports continued work towards efficient coupled model optimization and testing.

5.2 Shifted snowmelt seasonality impacts streamflow regimes for Yukon

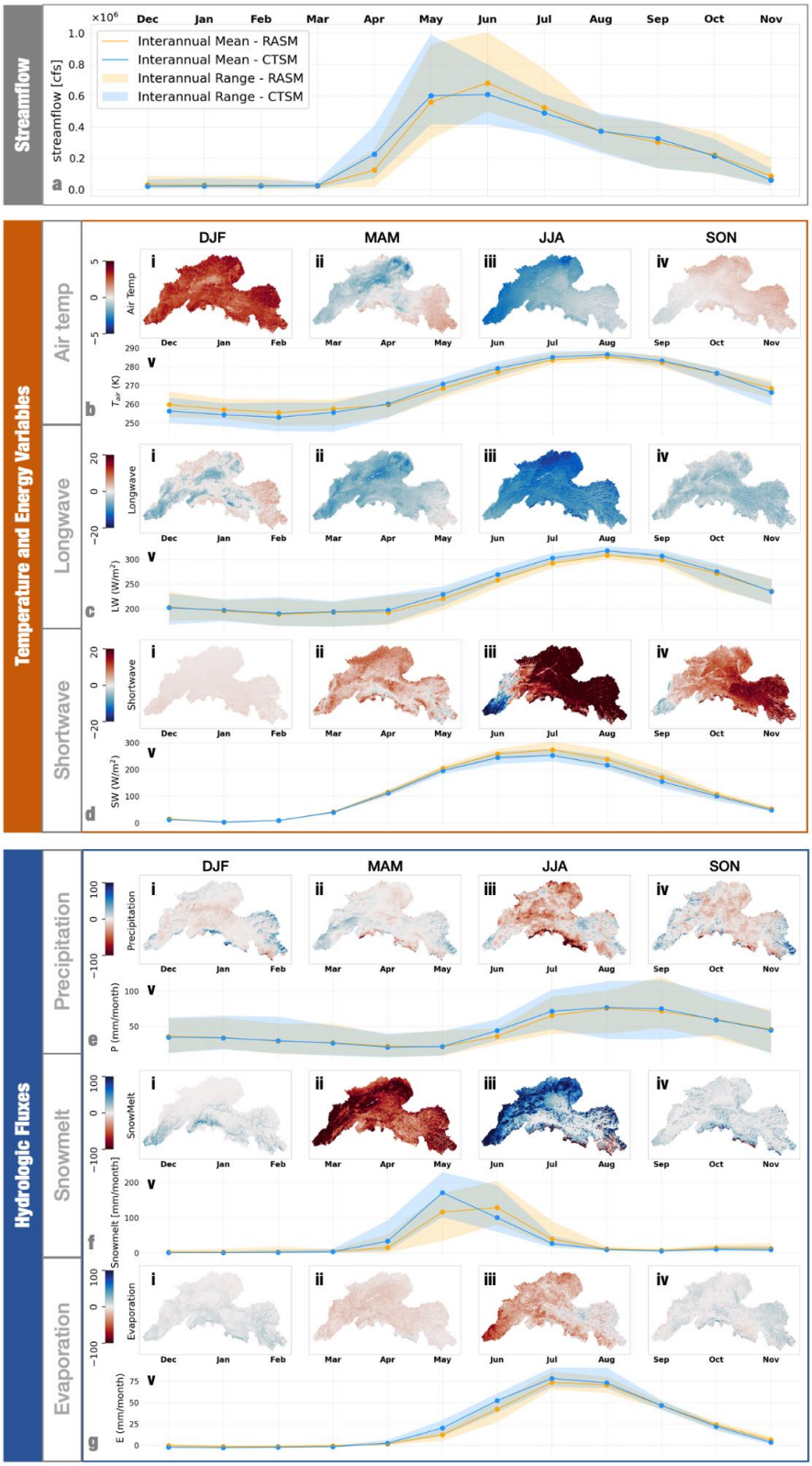

Figure 10. Differences between the meteorology simulated by RASM and the meteorological forcings used for standalone CTSM optimization. Panel a shows the mean monthly streamflow in RASM (yellow) and CTSM (blue). In Panels *b*, *c*, *d*, *e*, *f*, and *g*, sub-panels *i*, *ii*, *iii*, and *iv* show the mean seasonal discrepancies between RASM meteorology and CTSM meteorological forcings for winter, spring, summer, and fall, respectively. Sub-panels *v* show the mean monthly meteorological variables for RASM and CTSM.

The overall streamflow quantity was similar in RASM and CTSM, despite RASM having a slight negative precipitation bias. To examine the impacts of meteorological conditions and potential biases on streamflow simulations, the largest USGS gaged basin in Alaska, Yukon River at Pilot Station, was chosen as an exemplar. Both RASM and CTSM show a mean annual streamflow of 250 thousand cubic feet per second (cfs). However, the precipitation rate used to force CTSM has a higher regional average value of 540.6 mm/year compared to the simulated precipitation in RASM, which has a regional average value of 526.0 mm/year. This discrepancy is particularly evident in July and August. Simultaneously, CTSM simulates higher evapotranspiration (ET) during warm seasons with a regional average of 289.8 mm/year, higher than RASM with a regional average ET of 273.5 mm/year. Despite the positive precipitation bias, the impact of higher ET in CTSM likely compensates for the higher precipitation rate and contributes to the comparable overall streamflow quantities observed in both models.

A delayed timing of peak streamflow in RASM is primarily driven by later snowmelt compared to CTSM. In CTSM, the streamflow simulations peak in May with a higher volume observed in April and May (Figure *10a*) when compared to RASM. However, RASM exhibits a later yet higher peak streamflow volume compared to CTSM. In cold regions, such as our study area, the primary sources of runoff are precipitation, snowmelt, and glacier melt. From Figures *10e,v* and *10f,v*, it is evident that the discrepancies in streamflow regimes between RASM and CTSM are mainly attributed to an earlier onset of snowmelt in CTSM, with precipitation playing a relatively insignificant role. Additionally, the timing and intensity of snowmelt are significantly influenced by shortwave radiation, longwave radiation, and air temperatures. Based on Figures *10b,ii* and *10c,ii*, the spring air temperature and longwave radiation in RASM simulation are both lower than those used in CTSM. These differences drive a lower snowmelt in RASM compared to CTSM, contributing to the delayed peak streamflow timing observed in RASM.

5.3 Climate sensitivity

RASM and CTSM exhibit comparable runoff sensitivities to precipitation (θ_P) and these values are generally higher than those in ERA5 in 14 out of 15 major river basins (Figure 11). The mean values of θ_P across all basins are 0.70, 0.70, and 0.39 for RASM, CTSM, and ERA5 respectively, indicating that both RASM and CTSM show stronger responses of runoff to changes in precipitation compared to ERA5. The only exception is the Sagavanirktok River Basin, where θ_P is 0.91 for CTSM, slightly higher than RASM (0.76) and ERA5 (0.90). The observed mean value of θ_P across the same 15 basins is 0.74 (Cheng et al., 2023), indicating RASM and CTSM more realistically capture the climate sensitivity compared to ERA5. The lower θ_P can be attributed to the underestimated runoff to precipitation ratios (R/P ratio) in ERA5 compared to RASM and CTSM. For instance, across the entire Yukon River Basin, the R/P ratios in RASM and CTSM are both 0.47, while it is only 0.31 for ERA5. However, in the

Sagavanirktok River Basin, the R/P ratio in ERA5 is 0.66, higher than RASM (0.61) and CTSM (0.62).

Larger uncertainties exist in runoff sensitivities to air temperatures (θ_T) compared to θ_P. In RASM, CTSM, and ERA5, the median absolute value of the correlation coefficient ρ_P across all basins is 0.86, 0.88, and 0.45, respectively. These values are generally higher than the median absolute value of ρ_T, which are 0.28, 0.28, and 0.17, respectively. The higher correlation coefficient ρ_P indicates a more reliable response of runoff to precipitation compared to air temperatures.

ERA5 generally exhibits opposite runoff sensitivities to air temperature compared to RASM and CTSM. In ERA5, 10 basins show negative sensitivity with median values of -0.014 mm·day^{-1}·°C^{-1}, implying higher air temperatures might reduce runoff generation. However, in RASM and CTSM, only three basins show negative sensitivity, with median values of 0.033 mm·day^{-1}·°C^{-1} and 0.038 mm·day^{-1}·°C^{-1}, respectively. This means that, for a majority of the basins in RASM and CTSM, higher air temperatures are associated with increased runoff. A total of 7 out of 15 basins shows opposite runoff sensitivities between ERA5 and RASM and CTSM. In Cheng et al. (2023), θ_T were calculated using observed flows from USGS and the median value of θ_T across the same basins is 0.041 mm·day^{-1}·°C^{-1}, indicating that RASM and CTSM better capture the runoff sensitivity to air temperature compared to ERA5.

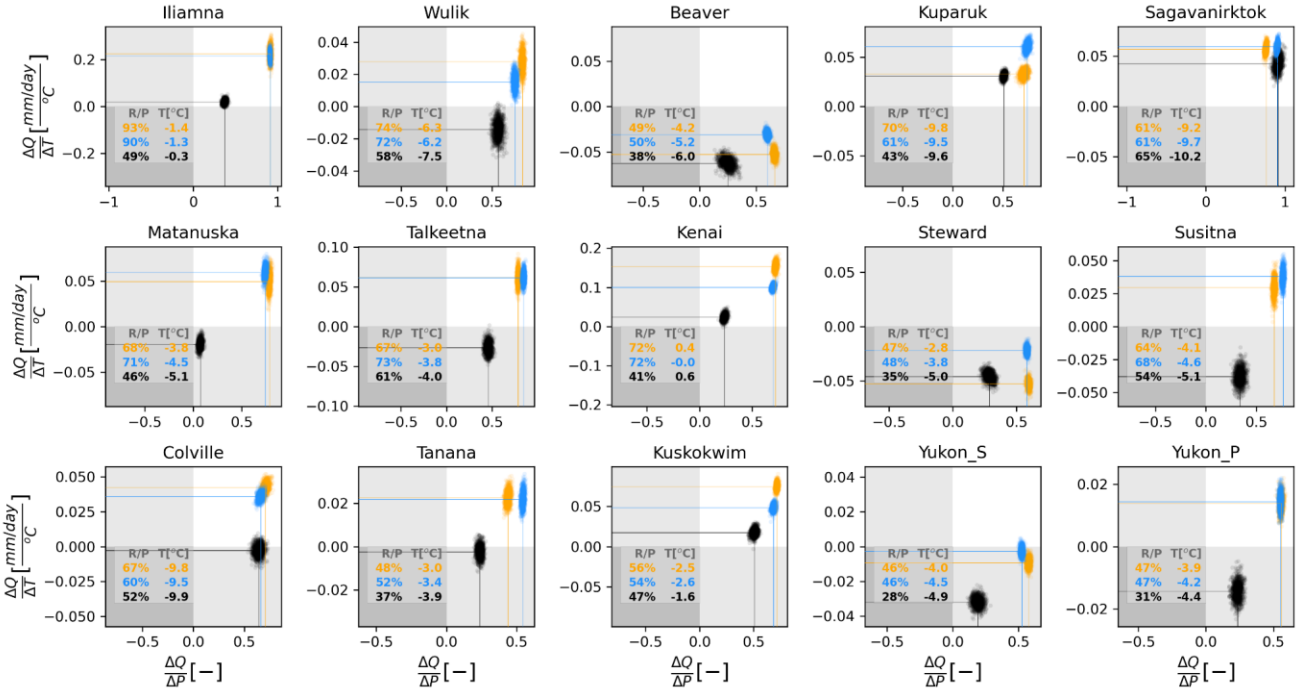

Figure 11. A climate sensitivity analysis for CTSM, RASM and ERA5, denoted by blue, orange, and black colors respectively. The x-axis denotes the rate of basin-averaged runoff change with precipitation change (θ_P), and the y-axis denotes the rate of basin-averaged runoff change with air temperature change (θ_T). In each subplot, the lower left table shows the basin-wide average runoff to precipitation ratio (R/P, %), and air temperature (T, °C).

5.4 The connectivity among hydrologic and energy fluxes varies among ERA5, CTSM, and RASM

To better understand process interdependencies in the three model configurations we computed the pairwise process connectivity with the transfer entropy measure as outlined in section 4.2. The resulting analysis is summarized in Figure 12 as a chord diagram, which shows the directional reduction in uncertainty for a variable given some knowledge of another. We say that processes "receive" more information when the transfer entropy is higher, meaning that the target variable's uncertainty is reduced if we know the value of the source variable. It is worth noting that the widths of the chords between diagrams is not directly comparable because the total information exchange is normalized by the circular visualization.

In RASM, the three temperature and energy variables, namely air temperature, longwave, and shortwave radiation, receive more information compared to CTSM and ERA5. Specifically, these variables receive 9.4%, 4.2%, and 3.0% of the transferred information for all pairs of selected variables in RASM, CTSM, and ERA5, as shown in Figure 12. The information transferred from ΔSWE and precipitation to longwave radiation is notably stronger in RASM compared to CTSM. This can be attributed to RASM's ability to account for land feedback to the atmosphere, explicitly capturing the influence of hydrologic fluxes on the energy balance.

Shortwave radiation and canopy evapotranspiration exchange information in RASM, significant at 99% confidence level, while these two variables exchange little information in CTSM and ERA5. The impact of shortwave radiation on canopy evapotranspiration is evident, while RASM dynamically captures the impacts of canopy evapotranspiration and soil moisture on atmospheric vapor pressure and therefore cloud formation, which consequently affects the shortwave radiation. This feedback is not seen in ERA5 or CTSM.

Snowmelt significantly contributes to runoff generation in RASM and CTSM while its contribution is minimally evident in ERA5. Similarly, precipitation affects runoff in RASM and CTSM whereas its impact is minimal in ERA5. These findings suggest that the runoff in ERA5 is predominantly influenced by subsurface processes, with precipitation and snowmelt as two major surface hydrologic fluxes playing a minor role in direct runoff generation. To investigate this hypothesis, we partition the total runoff to surface runoff and subsurface runoff. The results show that in ERA5, surface runoff only contributes to 20.8% of the total runoff. In contrast, in RASM and CTSM, surface runoff accounts for 83.7% and 80.6% of the total runoff, respectively. This substantial discrepancy in runoff partitioning explains the variation in process information transfer to runoff generation.

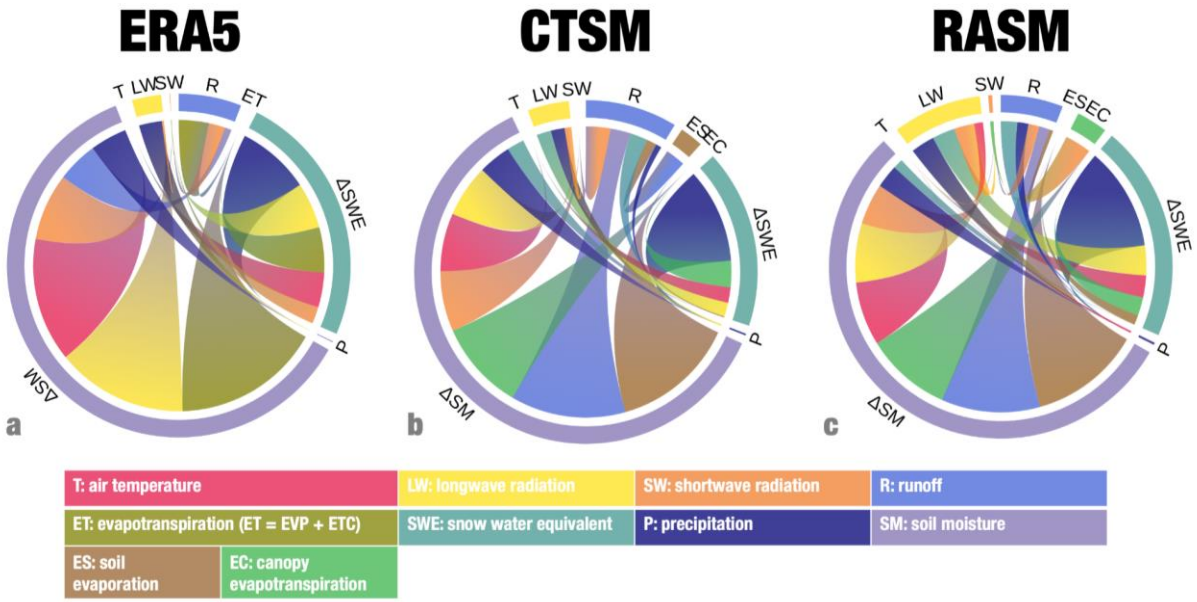

Figure 12. Transfer Entropy for ERA5 dataset, CTSM, and RASM. The outer circle is composed of arcs whose relative lengths correspond to the sum of information received from other sources. The inner sections are composed of chords, or ribbons, which indicate the direction and magnitude of information transfer.

6 Discussion

This study provides a 30-year 4 km historical regional climate simulation and comprehensive evaluation for Alaska and the Yukon River Basin. This is the first study using CTSM as the land component in RASM. We evaluated near-surface air temperature and four hydroclimate variables—precipitation, snowfall fraction, E/P ratio, and streamflow—against multiple observational datasets, assessing the performance of our RASM configuration for both hydroclimate and terrestrial hydrology. Specifically, RASM slightly overpredicted mean annual precipitation with a median relative bias of 14.4% and 16.7% compared to PNWNAmet and GPCP respectively (Table 3). The high Spearman rank-order correlation coefficients indicate well-simulated spatial patterns of precipitation (Table 3). Larger biases are observed in the spring season as well as in specific regions, particularly in the southern coastal mountains, including Denali, and the northern mountains (Figure 5). The seasonality of air temperature is slightly dampened in RASM, and the seasonal biases show spatial heterogeneity (Figure 6). Overestimation of winter air temperature is prominent in the north, southeast interior Alaska, and the Yukon headwaters while underestimation in summer air temperature is evident in north and west coasts of Alaska. Compared to ERA5, RASM simulates comparable quantity and seasonality of snowfall fraction and E/P ratios, and includes complex spatial patterns due to topography. While streamflow simulation in RASM generally performs well as compared to the standalone CTSM optimization, discrepancies arise during warm periods because the meteorology simulated in RASM differs from the meteorological forcing used for CTSM optimization. Compared to other large regional land-atmosphere coupled regional climate simulations, the amount of effort focused on surface hydrology simulation and performance improvement is to our knowledge unprecedented.

Our results highlight a remaining challenge to maintain the fidelity for both hydroclimate and terrestrial hydrology simultaneously in regional climate modeling. In previous studies, optimization of regional climate models successfully improved the simulated representation of the atmospheric water cycle in the pan-arctic region (Wei et al., 2002) and reduced summer warm biases in Europe (Bellprat et al., 2016). Comparatively, optimization of the terrestrial hydrologic cycle, especially runoff, is rare. This study, for the first time, incorporates an objective optimization of land parameters for streamflow and snow in a multi-decadal regional climate simulation. We show robust model performance as compared to the standalone land model. We present two precautionary measures to reduce the chance that our land model optimization deteriorates the coupled model. Nevertheless, the impacts of land parameters on land-atmosphere interactions, especially the connectivity among hydrologic and energy fluxes, remain unclear and are worth further investigation.

The runoff sensitivity to precipitation (θ_P) shows a reliable monotonic relationship, indicating higher precipitation leads to increased runoff. In the Yukon River Basin, both RASM and CTSM exhibit a similar θ_P value of 0.7 while ERA5 shows a much smaller θ_P, which is attributed to an underestimated runoff in ERA5. Moreover, we found that surface runoff contributes to over 80% of total runoff in RASM and CTSM, but only accounts for 21% of total runoff in ERA5. The underestimation of ERA5 runoff in Alaska is likely attributed to an underestimation of surface runoff.

The low reliability of climate sensitivity to temperatures may be attributed to the nonlinear response of runoff generation to temperature changes in cold regions. Runoff generation is regulated by air temperatures through intricate land processes, including snow accumulation, the timing and quantity of snowmelt, as well as the partition of precipitation to runoff and evapotranspiration. With warming, changes in evapotranspiration from soil, canopy, and snow can offset the influence of increasing precipitation (Newman et al., 2021), leading to larger uncertainties in runoff generation.

Finally, the two-way interactions between land and atmosphere in RASM are visualized through the transfer entropy among hydrologic and surface energy fluxes. The model's feedback from the land surface to the atmospheres enables it to capture the impacts of hydrologic fluxes on surface energy variables, resulting in a higher amount of information received by energy variables in RASM compared to CTSM or ERA5. Despite the presence of limitations, this analysis serves as an illustration to demonstrate the different connectivity among pairs of hydrologic and surface energy variables for RASM, CTSM, and ERA5. It is important to note that we only calculated lag-1 day transfer entropy over the aggregated Yukon basin, but the connectivity between variables can be strong at different spatial and temporal scales. Furthermore, we used a simple single-variate approach, and the multivariate process connectivity is not presented in this study. Last but not least, the spatial aggregation over a large domain smooths the time series that can affect the connectivity between variables. For example, in ERA5, shortwave radiation and air temperatures should theoretically affect ET, but it did not show up in this analysis. Future research could identify timing differences for process connectivity, explore multivariable approaches, and investigate more effective sampling methods over a large domain to gain a deeper and more comprehensive understanding and improve model fidelity.

7 Conclusion

To provide a high-fidelity hydroclimate and terrestrial hydrology simulation for Alaska, we leveraged offline land model optimization (Cheng et al., 2023) and iterative testing to improve RASM simulation. We then conducted a multi-decade simulation (1990-2021) at 4 km grid spacing using the optimized CTSM, which is novel for large domain regional climate modeling. Our study marks the first coupling of the CTSM land model into RASM. Evaluated against multiple observational datasets, this simulation well captures the climate statistics and spatial distributions of five hydroclimate and terrestrial hydrologic variables, including precipitation, air temperature, snow fraction, evaporation-to-precipitation ratios, and streamflow. Simulated precipitation shows major wet bias during the spring season and mostly in northern slopes and mountainous regions. Simulated air temperatures exhibit compressed seasonality with warm biases in winter and cold biases in summer.

Process oriented analyses reveal the drivers of streamflow discrepancies and process connectivity between offline CTSM and coupled RASM simulations. Compared to CTSM, lower spring air temperature and longwave radiation simulated by RASM leads to a slower spring snowmelt, contributing to a delayed timing of peak streamflow in the Yukon River. In both RASM and CTSM, higher precipitation generally leads to increased runoff while the relationship between air temperature and runoff exhibits large uncertainty, which can be attributed to the nonlinear response of runoff generation to temperature changes in cold regions. In addition, by utilizing information theory, we assessed the feedback from the land surface to the atmosphere in RASM by finding a higher amount of information received by temperature and energy variables in RASM compared to CTSM.

Acknowledgement

The high-resolution climate dataset is archived on the National Science Foundation (NSF) National Center for Atmospheric Research (NCAR) Research Data Archive (RDA) and can be accessed through this following DOI, 10.5065/ZPSB-PS82. This project was funded by NSF Navigating the New Arctic Grant 1928078 and supported by the NSF NCAR, which is a major facility sponsored by the National Science Foundation under Cooperative Agreement No. 1852977. We would like to acknowledge high-performance computing support from Cheyenne (https://doi-org.cuucar.idm.oclc.org/10.5065/D6RX99HX) provided by NCAR's Computational and Information Systems Laboratory, sponsored by the National Science Foundation. We thank our Indigenous Advisory Council and numerous Tribal and First Nation decision-makers for providing important insights to help inform the RASM configuration design. Additionally, we greatly benefited from the following open-source libraries to perform analyses presented in this study: NumPy (Van Der Walt et al., 2011), pandas (McKinney, 2010), geopandas (Jordahl et al., 2020), xarray (Hoyer & Hamman, 2017), matplotlib (Hunter, 2007), and cartopy (Met Office, 2015).

Reference

Adler, R. F., Huffman, G. J., Chang, A., Ferraro, R., Xie, P.-P., Janowiak, J., Rudolf, B., Schneider, U., Curtis, S., Bolvin, D., Gruber, A., Susskind, J., Arkin, P., & Nelkin, E. (2003). The Version-2 Global Precipitation Climatology Project (GPCP) Monthly Precipitation Analysis (1979–Present). *Journal of Hydrometeorology*, *4*(6), 1147–1167. https://doi.org/10.1175/1525-7541(2003)004<1147:TVGPCP>2.0.CO;2

Akperov, M., Rinke, A., Mokhov, I. I., Semenov, V. A., Parfenova, M. R., Matthes, H., Adakudlu, M., Boberg, F., Christensen, J. H., Dembitskaya, M. A., Dethloff, K., Fettweis, X., Gutjahr, O., Heinemann, G., Koenigk, T., Koldunov, N. V., Laprise, R., Mottram, R., Nikiéma, O., … Zhang, W. (2019). Future projections of cyclone activity in the Arctic for the 21st century from regional climate models (Arctic-CORDEX). *Global and Planetary Change*, *182*, 103005. https://doi.org/10.1016/j.gloplacha.2019.103005

Behrangi, A., Christensen, M., Richardson, M., Lebsock, M., Stephens, G., Huffman, G. J., Bolvin, D., Adler, R. F., Gardner, A., Lambrigtsen, B., & Fetzer, E. (2016). Status of high-latitude precipitation estimates from observations and reanalyses. *Journal of Geophysical Research: Atmospheres*, *121*(9), 4468–4486. https://doi.org/10.1002/2015JD024546

Bellprat, O., Kotlarski, S., Lüthi, D., Elía, R. D., Frigon, A., Laprise, R., & Schär, C. (2016). Objective Calibration of Regional Climate Models: Application over Europe and North America. *Journal of Climate*, *29*(2), 819–838. https://doi.org/10.1175/JCLI-D-15-0302.1

Bellprat, O., Kotlarski, S., Lüthi, D., & Schär, C. (2012). Objective calibration of regional climate models. *Journal of Geophysical Research: Atmospheres*, *117*(D23). https://doi.org/10.1029/2012JD018262

Bennett, A., Nijssen, B., Ou, G., Clark, M., & Nearing, G. (2019). Quantifying Process Connectivity With Transfer Entropy in Hydrologic Models. *Water Resources Research*, *55*(6), 4613–4629. https://doi.org/10.1029/2018WR024555

Berg, P., Wagner, S., Kunstmann, H., & Schädler, G. (2013). High resolution regional climate model simulations for Germany: Part I—validation. *Climate Dynamics*, *40*(1), 401–414. https://doi.org/10.1007/s00382-012-1508-8

Bieniek, P. A., Walsh, J. E., Thoman, R. L., & Bhatt, U. S. (2014). Using Climate Divisions to Analyze Variations and Trends in Alaska Temperature and Precipitation. *Journal of Climate*, *27*(8), 2800–2818. https://doi.org/10.1175/JCLI-D-13-00342.1

Blaskey, D., Koch, J. C., Gooseff, M. N., Newman, A. J., Cheng, Y., O'Donnell, J. A., & Musselman, K. N. (2023). Increasing Alaskan river discharge during the cold season is driven by recent warming. *Environmental Research Letters*, *18*(2), 024042. https://doi.org/10.1088/1748-9326/acb661

Bukovsky, M. S., Carrillo, C. M., Gochis, D. J., Hammerling, D. M., McCrary, R. R., & Mearns, L. O. (2015). Toward Assessing NARCCAP Regional Climate Model Credibility for the North American Monsoon: Future Climate Simulations. *Journal of Climate*, *28*(17), 6707–6728. https://doi.org/10.1175/JCLI-D-14-00695.1

Cassano, J. J., DuVivier, A., Roberts, A., Hughes, M., Seefeldt, M., Brunke, M., Craig, A., Fisel, B., Gutowski, W., Hamman, J., Higgins, M., Maslowski, W., Nijssen, B., Osinski, R., & Zeng, X. (2017). Development of the Regional Arctic System Model (RASM): Near-Surface Atmospheric Climate Sensitivity. *Journal of Climate*, *30*(15), 5729–5753. https://doi.org/10.1175/JCLI-D-15-0775.1

Cheng, Y., Craig, A., Musselman, K., & Newman, A. (2024). *Multi-decadal historical regional hydroclimate simulation with two mid 21st century Pseudo-Global Warming futures over Alaska and the Yukon at 4 km resolution* [netCDF]. Research Data Archive at the National Center for Atmospheric Research, Computational and Information Systems Laboratory. https://doi.org/10.5065/ZPSB-PS82

Cheng, Y., Swenson, S., Hamman, J., Dagon, K., Kennedy, D., Newman, A. J., Lawrence, D., & Musselman, K. N. (2023). Moving Land Models Toward More Actionable Science: A Novel Application of the Community Terrestrial Systems Model Across Alaska and the Yukon River Basin. *Water Resources Research*, *59*(1), e2022WR032204. https://doi.org/10.1029/2022WR032204

Couvreux, F., Hourdin, F., Williamson, D., Roehrig, R., Volodina, V., Villefranque, N., Rio, C., Audouin, O., Salter, J., Bazile, E., Brient, F., Favot, F., Honnert, R., Lefebvre, M.-P., Madeleine, J.-B., Rodier, Q., & Xu, W. (2021). Process-Based Climate Model Development Harnessing Machine Learning: I. A Calibration Tool for Parameterization Improvement. *Journal of Advances in Modeling Earth Systems*, *13*(3), e2020MS002217. https://doi.org/10.1029/2020MS002217

Cox, C. J., Stone, R. S., Douglas, D. C., Stanitski, D. M., Divoky, G. J., Dutton, G. S., Sweeney, C., George, J. C., & Longenecker, D. U. (2017). Drivers and Environmental Responses to the Changing Annual Snow Cycle of Northern Alaska. *Bulletin of the American Meteorological Society*, *98*(12), 2559–2577. https://doi.org/10.1175/BAMS-D-16-0201.1

Gudmundsson, L., Leonard, M., Do, H. X., Westra, S., & Seneviratne, S. I. (2019). Observed Trends in Global Indicators of Mean and Extreme Streamflow. *Geophysical Research Letters*, *46*(2), 756–766. https://doi.org/10.1029/2018GL079725

Gutowski Jr., W. J., Giorgi, F., Timbal, B., Frigon, A., Jacob, D., Kang, H.-S., Raghavan, K., Lee, B., Lennard, C., Nikulin, G., O'Rourke, E., Rixen, M., Solman, S., Stephenson, T., & Tangang, F. (2016). WCRP COordinated Regional Downscaling EXperiment (CORDEX): A diagnostic MIP for CMIP6. *Geoscientific Model Development*, *9*(11), 4087–4095. https://doi.org/10.5194/gmd-9-4087-2016

Hamman, J., Nijssen, B., Brunke, M., Cassano, J., Craig, A., DuVivier, A., Hughes, M., Lettenmaier, D. P., Maslowski, W., Osinski, R., Roberts, A., & Zeng, X. (2016). Land Surface Climate in the Regional Arctic System Model. *Journal of Climate*, *29*(18), 6543–6562. https://doi.org/10.1175/JCLI-D-15-0415.1

Hersbach, H., Bell, B., Berrisford, P., Hirahara, S., Horányi, A., Muñoz-Sabater, J., Nicolas, J., Peubey, C., Radu, R., Schepers, D., Simmons, A., Soci, C., Abdalla, S., Abellan, X., Balsamo, G., Bechtold, P., Biavati, G., Bidlot, J., Bonavita, M., … Thépaut, J.-N. (2020). The ERA5 global reanalysis. *Quarterly Journal of the Royal Meteorological Society*, *146*(730), 1999–2049. https://doi.org/10.1002/qj.3803

Hlaváčková-Schindler, K., Paluš, M., Vejmelka, M., & Bhattacharya, J. (2007). Causality detection based on information-theoretic approaches in time series analysis. *Physics Reports*, *441*(1), 1–46. https://doi.org/10.1016/j.physrep.2006.12.004

Hong, S.-Y., Noh, Y., & Dudhia, J. (2006). A New Vertical Diffusion Package with an Explicit Treatment of Entrainment Processes. *Monthly Weather Review*, *134*(9), 2318–2341. https://doi.org/10.1175/MWR3199.1

Hoyer, S., & Hamman, J. J. (2017). xarray: N-D labeled Arrays and Datasets in Python. *Journal of Open Research Software*, *5*(1). https://doi.org/10.5334/JORS.148

Hunter, J. D. (2007). Matplotlib: A 2D Graphics Environment. *Computing in Science & Engineering*, *9*(03), 90–95. https://doi.org/10.1109/MCSE.2007.55

Jakob, C. (2010). Accelerating Progress in Global Atmospheric Model Development through Improved Parameterizations: Challenges, Opportunities, and Strategies. *Bulletin of the American Meteorological Society*, *91*(7), 869–876. https://doi.org/10.1175/2009BAMS2898.1

Janić, Z. I. (2001). *Nonsingular implementation of the Mellor-Yamada level 2.5 scheme in the NCEP Meso model* (Office Note (National Centers for Environmental Prediction (U.S.)) ; 437). National Centers for Environmental Prediction (U.S.). https://repository.library.noaa.gov/view/noaa/11409

Jordahl, K., den Bossche, J. V., Fleischmann, M., Wasserman, J., McBride, J., Gerard, J., Tratner, J., Perry, M., Badaracco, A. G., Farmer, C., Hjelle, G. A., Snow, A. D., Cochran, M., Gillies, S., Culbertson, L., Bartos, M., Eubank, N., Maxalbert, Bilogur, A., … Leblanc, F. (2020). *geopandas/geopandas: V0.8.1*. https://doi.org/10.5281/ZENODO.3946761

Jorgenson, M. T., Shur, Y. L., & Pullman, E. R. (2006). Abrupt increase in permafrost degradation in Arctic Alaska. *Geophysical Research Letters*, *33*(2). https://doi.org/10.1029/2005GL024960

Kennedy, D., Dagon, K., Lawrence, D. M., Fisher, R. A., Sanderson, B. M., Collier, N., Hoffman, F., Koven, C. D., Kluzek, E., Levis, S., Lu, X., Oleson, K. W., Zarakas, C. M., Cheng, Y., Foster, A. C., Fowler, M. D., Hawkins, L. R., Kavoo, T., Kumar, S., … Wood, A. W. (n.d.). The Community Land Model, version 5.1 One-at-a-time Parameter Perturbation Ensemble. *Manuscript in Preparation*.

Kennedy, D., Swenson, S., Oleson, K. W., Lawrence, D. M., Fisher, R., Lola da Costa, A. C., & Gentine, P. (2019). Implementing Plant Hydraulics in the Community Land Model, Version 5. *Journal of Advances in Modeling Earth Systems*, *11*(2), 485–513. https://doi.org/10.1029/2018MS001500

Knoben, W. J. M., Freer, J. E., & Woods, R. A. (2019). Technical note: Inherent benchmark or not? Comparing Nash–Sutcliffe and Kling–Gupta efficiency scores. *Hydrology and Earth System Sciences*, *23*(10), 4323–4331. https://doi.org/10.5194/hess-23-4323-2019

Knoll, L. B., Sharma, S., Denfeld, B. A., Flaim, G., Hori, Y., Magnuson, J. J., Straile, D., & Weyhenmeyer, G. A. (2019). Consequences of lake and river ice loss on cultural ecosystem services. *Limnology and Oceanography Letters*, *4*(5), 119–131. https://doi.org/10.1002/LOL2.10116

Lawrence, D. M., Fisher, R. A., Koven, C. D., Oleson, K. W., Swenson, S. C., Bonan, G., Collier, N., Ghimire, B., van Kampenhout, L., Kennedy, D., Kluzek, E., Lawrence, P. J., Li, F., Li, H., Lombardozzi, D., Riley, W. J., Sacks, W. J., Shi, M., Vertenstein, M., … Zeng, X. (2019). The Community Land Model Version 5: Description of New Features, Benchmarking, and Impact of Forcing Uncertainty. *Journal of Advances in Modeling Earth Systems*, *11*(12), 4245–4287. https://doi.org/10.1029/2018MS001583

Lawrence, D. M., & Slater, A. G. (2005). A projection of severe near-surface permafrost degradation during the 21st century. *Geophysical Research Letters*, *32*(24), 1–5. https://doi.org/10.1029/2005GL025080

Li, Y., Li, Z., Zhang, Z., Chen, L., Kurkute, S., Scaff, L., & Pan, X. (2019). High-resolution regional climate modeling and projection over western Canada using a weather research

forecasting model with a pseudo-global warming approach. *Hydrology and Earth System Sciences*, *23*(11), 4635–4659. https://doi.org/10.5194/hess-23-4635-2019

Maraun, D. (2012). Nonstationarities of regional climate model biases in European seasonal mean temperature and precipitation sums. *Geophysical Research Letters*, *39*(6). https://doi.org/10.1029/2012GL051210

Marschinski, R., & Kantz, H. (2002). Analysing the information flow between financial time series. *The European Physical Journal B - Condensed Matter and Complex Systems*, *30*(2), 275–281. https://doi.org/10.1140/epjb/e2002-00379-2

McKinney, W. (2010). Data Structures for Statistical Computing in Python. *THE 9th PYTHON IN SCIENCE CONFERENCE*, 56–61. https://doi.org/10.25080/MAJORA-92BF1922-00A

McNeeley, S. M., & Shulski, M. D. (2011). Anatomy of a closing window: Vulnerability to changing seasonality in Interior Alaska. *Global Environmental Change*, *21*(2), 464–473. https://doi.org/10.1016/j.gloenvcha.2011.02.003

Mearns, L. O., McGinnis, S., Korytina, D., Arritt, R., Biner, S., Bukovsky, M., Chang, H.-I., Christensen, O., Herzmann, D., Jiao, Y., Kharin, S., Lazare, M., Nikulin, G., Qian, M., Scinocca, J., Winger, K., Castro, C., Frigon, A., & Gutowski, W. (2017). *The NA-CORDEX dataset (1.0)* (1.0) [dataset]. https://doi.org/10.5065/D6SJ1JCH

Met Office. (2015). *Cartopy: A cartographic python library with a matplotlib interface*.

Mizukami, N., Clark, M. P., Sampson, K., Nijssen, B., Mao, Y., McMillan, H., Viger, R. J., Markstrom, S. L., Hay, L. E., Woods, R., Arnold, J. R., & Brekke, L. D. (2016). MizuRoute version 1: A river network routing tool for a continental domain water

resources applications. *Geoscientific Model Development*, *9*(6), 2223–2228. https://doi.org/10.5194/GMD-9-2223-2016

Monaghan, A. J., Clark, M. P., Barlage, M. P., Newman, A. J., Xue, L., Arnold, J. R., & Rasmussen, R. M. (2018). High-Resolution Historical Climate Simulations over Alaska. *Journal of Applied Meteorology and Climatology*, *57*(3), 709–731. https://doi.org/10.1175/JAMC-D-17-0161.1

Moriasi, D. N., Gitau, M. W., Pai, N., & Daggupati, P. (2015). Hydrologic and Water Quality Models: Performance Measures and Evaluation Criteria. *Transactions of the ASABE*, *58*(6), 1763–1785. https://doi.org/10.13031/TRANS.58.10715

Musselman, K. N., Addor, N., Vano, J. A., & Molotch, N. P. (2021). Winter melt trends portend widespread declines in snow water resources. *Nature Climate Change*, *11*(5), Article 5. https://doi.org/10.1038/s41558-021-01014-9

Newman, A. J., Clark, M. P., Wood, A. W., & Arnold, J. R. (2020). Probabilistic Spatial Meteorological Estimates for Alaska and the Yukon. *Journal of Geophysical Research: Atmospheres*, *125*(22), e2020JD032696. https://doi.org/10.1029/2020JD032696

Newman, A. J., Monaghan, A. J., Clark, M. P., Ikeda, K., Xue, L., Gutmann, E. D., & Arnold, J. R. (2021). Hydroclimatic changes in Alaska portrayed by a high-resolution regional climate simulation. *Climatic Change*, *164*(1–2), 1–21. https://doi.org/10.1007/S10584-021-02956-X/FIGURES/12

Osterkamp, T. E., & Romanovsky, V. E. (1999). Evidence for warming and thawing of discontinuous permafrost in Alaska. *PERMAFROST AND PERIGLACIAL PROCESSES*, *10*, 17–37.

Papadimitriou, L. V., Koutroulis, A. G., Grillakis, M. G., & Tsanis, I. K. (2017). The effect of GCM biases on global runoff simulations of a land surface model. *Hydrology and Earth System Sciences*, *21*(9), 4379–4401. https://doi.org/10.5194/hess-21-4379-2017

Rasmussen, R., Chen, F., Liu, C. H., Ikeda, K., Prein, A., Kim, J., Schneider, T., Dai, A., Gochis, D., Dugger, A., Zhang, Y., Jaye, A., Dudhia, J., He, C., Harrold, M., Xue, L., Chen, S., Newman, A., Dougherty, E., … Miguez-Macho, G. (2023). CONUS404: The NCAR-USGS 4-km long-term regional hydroclimate reanalysis over the CONUS. *Bulletin of the American Meteorological Society*, *1*(aop). https://doi.org/10.1175/BAMS-D-21-0326.1

Saito, K., Machiya, H., Iwahana, G., Ohno, H., & Yokohata, T. (2020). Mapping simulated circum-Arctic organic carbon, ground ice, and vulnerability of ice-rich permafrost to degradation. *Progress in Earth and Planetary Science*, *7*(1), 1–15. https://doi.org/10.1186/S40645-020-00345-Z/FIGURES/7

Schär, C., Frei, C., Lüthi, D., & Davies, H. C. (1996). Surrogate climate-change scenarios for regional climate models. *Geophysical Research Letters*, *23*(6), 669–672. https://doi.org/10.1029/96GL00265

Schreiber, T. (2000). Measuring Information Transfer. *Physical Review Letters*, *85*(2), 461–464. https://doi.org/10.1103/PhysRevLett.85.461

Skamarock, C., Klemp, B., Dudhia, J., Gill, O., Barker, D., Duda, G., Huang, X., Wang, W., & Powers, G. (2008). *A Description of the Advanced Research WRF Version 3*. https://doi.org/10.5065/D68S4MVH

Stafford, J. M., Wendler, G., & Curtis, J. (2000). Temperature and precipitation of Alaska: 50 year trend analysis. *Theoretical and Applied Climatology*, *67*(1), 33–44. https://doi.org/10.1007/s007040070014

Stone, R. S., Dutton, E. G., Harris, J. M., & Longenecker, D. (2002). Earlier spring snowmelt in northern Alaska as an indicator of climate change. *Journal of Geophysical Research: Atmospheres*, *107*(D10), ACL 10-1. https://doi.org/10.1029/2000JD000286

Tapiador, F. J., Navarro, A., Moreno, R., Sánchez, J. L., & García-Ortega, E. (2020). Regional climate models: 30 years of dynamical downscaling. *Atmospheric Research*, *235*, 104785. https://doi.org/10.1016/j.atmosres.2019.104785

Van Der Walt, S., Colbert, S. C., & Varoquaux, G. (2011). The NumPy array: A structure for efficient numerical computation. *Computing in Science and Engineering*, *13*(2), 22–30. https://doi.org/10.1109/MCSE.2011.37

Van Tiel, M., Van Loon, A. F., Seibert, J., & Stahl, K. (2021). Hydrological response to warm and dry weather: Do glaciers compensate? *Hydrology and Earth System Sciences*, *25*(6), 3245–3265. https://doi.org/10.5194/hess-25-3245-2021

Wang, C., Duan, Q., Gong, W., Ye, A., Di, Z., & Miao, C. (2014). An evaluation of adaptive surrogate modeling based optimization with two benchmark problems. *Environmental Modelling & Software*, *60*, 167–179. https://doi.org/10.1016/J.ENVSOFT.2014.05.026

Wei, H., Gutowski, W. J., Vorosmarty, C. J., & Fekete, B. M. (2002). Calibration and Validation of a Regional Climate Model for Pan-Arctic Hydrologic Simulation. *Journal of Climate*, *15*(22), 3222–3236. https://doi.org/10.1175/1520-0442(2002)015<3222:CAVOAR>2.0.CO;2

White, J. H. R., Walsh, J. E., & Thoman Jr, R. L. (2021). Using Bayesian statistics to detect trends in Alaskan precipitation. *International Journal of Climatology*, *41*(3), 2045–2059. https://doi.org/10.1002/joc.6946

Wood, A. W., Leung, L. R., Sridhar, V., & Lettenmaier, D. P. (2004). Hydrologic Implications of Dynamical and Statistical Approaches to Downscaling Climate Model Outputs. *Climatic Change 2004 62:1*, *62*(1), 189–216. https://doi.org/10.1023/B:CLIM.0000013685.99609.9E

Xue, L., Wang, Y., Newman, A. J., Ikeda, K., Rasmussen, R. M., Giambelluca, T. W., Longman, R. J., Monaghan, A. J., Clark, M. P., & Arnold, J. R. (2020). How will rainfall change over Hawai‘i in the future? High-resolution regional climate simulation of the Hawaiian Islands. *Bulletin of Atmospheric Science and Technology*, *1*(3), 459–490. https://doi.org/10.1007/s42865-020-00022-5